American Mineralogist, Volume 98, pages 870–878, 2013

Kangite, $(Sc,Ti,Al,Zr,Mg,Ca,\square)_2O_3$, a new ultra-refractory scandia mineral from the Allende meteorite: Synchrotron micro-Laue diffraction and electron backscatter diffraction

Chi Ma,[1,*] Oliver Tschauner,[1,2] John R. Beckett,[1] George R. Rossman,[1] and Wenjun Liu[3]

[1]Division of Geological and Planetary Sciences, California Institute of Technology, Pasadena, California 91125, U.S.A.
[2]High Pressure Science and Engineering Center and Department of Geoscience, University of Nevada, Las Vegas, Nevada 89154, U.S.A.
[3]Advanced Photon Source, Argonne National Laboratory, Argonne, Illinois 60439, U.S.A.

Abstract

Kangite (IMA 2011-092), $(Sc,Ti,Al,Zr,Mg,Ca,\square)_2O_3$, is a new scandia mineral, occurring as micrometer-sized crystals with REE-rich perovskite and spinel in a davisite-dominant ultra-refractory inclusion from the Allende CV3 carbonaceous chondrite. The phase was characterized by SEM, EBSD, synchrotron micro-Laue diffraction, micro-Raman, and EPMA. The mean chemical composition of the type kangite is (wt%) TiO_2 36.6, Sc_2O_3 26.4, ZrO_2 11.3, Al_2O_3 7.0, Y_2O_3 5.4, CaO 3.9, MgO 3.14, Dy_2O_3 1.8, SiO_2 1.7, V_2O_3 1.31, Er_2O_3 0.92, FeO 0.8, Gd_2O_3 0.60, Ho_2O_3 0.40, Tb_2O_3 0.18, Cr_2O_3 0.09, ThO_2 0.04, O –0.3, sum 101.28, which leads to an empirical formula calculated on the basis of 3 O atoms of $[(Sc_{0.54}Al_{0.16}Y_{0.07}V_{0.03}Gd_{0.01}Dy_{0.01}Er_{0.01})^{3+}_{\Sigma 0.83}(Ti_{0.66}Zr_{0.13})^{4+}_{\Sigma 0.79}(Mg_{0.11}Ca_{0.06}\ Fe_{0.02})^{2+}_{\Sigma 0.19}\square_{0.19}]_{\Sigma 2.00}O_3$. Synchrotron micro-Laue diffraction (i.e., an energy scan by a high-flux X-ray monochromatic beam) on one type domain at submicrometer resolution revealed that kangite has a cation-deficient $Ia\bar{3}$ bixbyite-type cubic structure. The cell parameters are $a = 9.842(1)$ Å, $V = 953.3(1)$ Å^3, $Z = 16$, which leads to a calculated density of 3.879 g/cm^3. Kangite is a new ultra-refractory mineral, likely originating through low-temperature oxidation of a Sc-,Ti^{3+}-enriched high-temperature condensate oxide dating to the birth of the Solar System.

Keywords: Kangite, $(Sc,Ti,Al,Zr,Mg,Ca,\square)_2O_3$, new ultra-refractory mineral, scandia, Allende meteorite, CV3 carbonaceous chondrite, synchrotron micro-Laue diffraction, EBSD, nano-mineralogy, REE

Introduction

During a nano-mineralogy investigation of a previously described inclusion, ACM-3, in the Allende meteorite (Ma and Rossman 2009b), a new ultra-refractory Sc-,Ti-rich mineral $(Sc,Ti,Al,Zr,Mg,Ca,\square)_2O_3$, named "kangite," was discovered. Electron probe microanalysis (EPMA), high-resolution scanning electron microscope (SEM), electron backscatter diffraction (EBSD), synchrotron micro-Laue diffraction with subsequent energy scans, and micro-Raman analyses were used to determine its composition, physical properties, and structure and to characterize associated phases. Synthetic Sc_2O_3 is well known but synthetic $(Sc,Ti,Al,Zr,Mg,Ca,\square)_2O_3$ is unknown. Kangite is a new mineral species and a phase new to meteoritics. In this paper, we describe the first occurrence of kangite in nature, as a new ultra-refractory oxide, among the oldest solid materials in the Solar System.

Mineral name and type material

The mineral and the mineral name (kangite) have been approved by the Commission on New Minerals, Nomenclature and Classification (CNMNC) of the International Mineralogical Association (IMA 2011-092). The name is derived from "kang," the Chinese word for the element scandium. Holotype material has been deposited under catalog USNM 7555 in the Smithsonian Institution's National Museum of Natural History, Washington D.C., U.S.A. Section USNM 7555 also contains type davisite (IMA 2008-030; Ma and Rossman 2009b).

Occurrence

The Allende meteorite fell in and near Pueblito de Allende, Chihuahua, Mexico on February 8, 1969 (Clarke et al. 1971). This CV3 carbonaceous chondrite is probably the most highly studied meteorite and the results of these studies have greatly influenced current thinking about processes, timing, and chemistry in the primitive solar nebula and in small planetary bodies. The mineral kangite was found within one irregular ultra-refractory inclusion, ACM-3, in one polished section (USNM 7555), prepared from a ~1 cm diameter Allende fragment (Caltech Meteorite Collection No. Allende12A). ACM-3 is about 130 μm in diameter in the section plane and is surrounded by a matrix of mostly fine-grained olivine and troilite. Kangite occurs interstitially, along with perovskite and spinel, within an aggregate of the type davisite crystals (Figs. 1–2). All four kangite grains are in contact with davisite and two are also in contact with perovskite. One was observed in contact with spinel.

Appearance, physical and optical properties

Kangite occurs as four irregular to subhedral grains, 1 to 4 μm in size, which constitute the type material (Fig. 2). In the optically thick section (150 μm in thickness), kangite is opaque.

* E-mail: chi@gps.caltech.edu

0003-004X/13/0506–870$05.00/DOI: http://dx.doi.org/10.2138/am.2013.4290

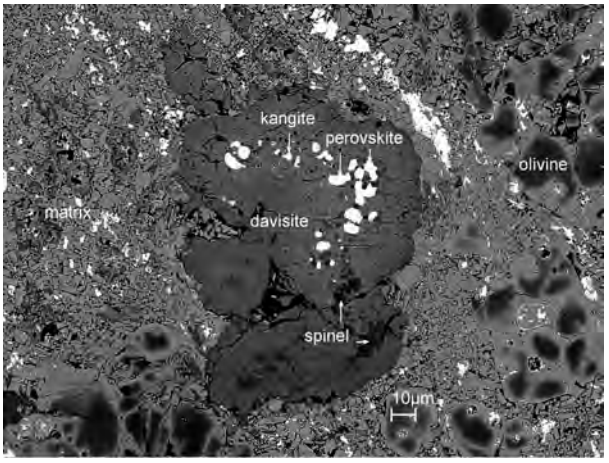

FIGURE 1. Backscatter electron (BSE) image of ultra-refractory inclusion ACM-3 in section USNM 7555 from the Allende meteorite, where the type davisite (Ma and Rossman 2009b) and kangite (this study) occur.

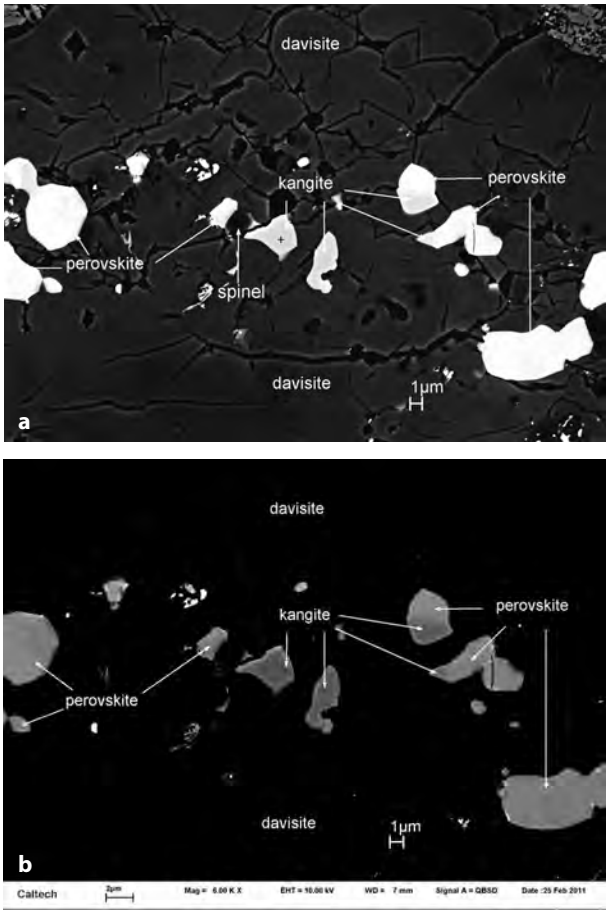

FIGURE 2. Enlarged BSE images of ACM-3 with contrasts optimized to show kangite microcrystals (type material) with perovskite and spinel in host davisite. The cross mark shown in panel **a** indicates where the EBSD pattern (shown in Fig. 6) and the synchrotron micro-Laue diffraction data were collected.

Color, streak, luster, hardness, tenacity, cleavage, fracture, density, and refractive index were not determined because of the small grain size. Given the large extent of solid solution in the natural material and its cation deficient stoichiometry, it is unlikely that these properties are close to those of synthetic Sc_2O_3. The density, calculated from its crystal structure and the empirical formula, is 3.879 g/cm^3, which is similar to those of Sc_2O_3 (3.86) and panguite (3.75), but lower than those of TiO_2 (4.59) and Ti_2O_3 (4.23). Kangite is not cathodoluminescent under the electron beam in an SEM and we observed no crystal forms or twinning. Visible light fluorescence can be excited by light of 514.5 nm; we did not check for fluorescence using alternative wavelengths.

CHEMICAL COMPOSITION

Chemical analyses of kangite (on the two leftmost grains in Fig. 2) and associated minerals were carried out using a JEOL 8200 electron microprobe (WDS: 15 kV; 5 nA and 25 nA; beam in focused mode) interfaced with the Probe for EPMA program from Probe Software, Inc. Possible interferences on peak position and background position were checked and corrected for all measured elements based on WDS scans and using Probe for EPMA; on-peak interferences of Ti$K\alpha$ by Sc; V$K\alpha$ by Ti and Y; Cr$K\alpha$ by V; Er$L\alpha$ by Tb; Ho$L\alpha$ by Gd; La$L\alpha$ by Nd; Ce$L\alpha$ by Ti and V; and Nd$L\alpha$ by Ce were corrected. Standards for the analysis were TiO_2 (Ti$K\alpha$, O$K\alpha$), $ScPO_4$ (Sc$K\alpha$), zircon (Zr$L\alpha$), anorthite (Ca$K\alpha$, Al$K\alpha$, Si$K\alpha$), YPO_4 (Y$L\alpha$), forsterite (Mg$K\alpha$), fayalite (Fe$K\alpha$), $DyPO_4$ (Dy$L\alpha$), $ErPO_4$ (Er$L\alpha$), $GdPO_4$ (Gd$L\alpha$), $TbPO_4$ (Tb$L\alpha$), $HoPO_4$ (Ho$L\alpha$), ThO_2 (ThMα), V_2O_3 (V$K\alpha$), Cr_2O_3 (Cr$K\alpha$), $LaPO_4$ (La$L\alpha$), $CePO_4$ (Ce$L\alpha$), $NdPO_4$ (Nd$L\alpha$), $SmPO_4$ (Sm$L\alpha$), and $YbPO_4$ (Yb$L\alpha$). Quantitative elemental microanalyses were processed with the CITZAF correction procedure (Armstrong 1995) and analytical results are given in Table 1. No other element with an atomic number exceeding 4 was detected by WDS scans at 15 kV, 25 nA, and 300 nA. In particular, none of the light rare earth elements (LREE) nor Yb was detected in kangite or in associated perovskite and davisite; detection limits for these elements at 99% confidence were 0.03 wt% for Sm and 0.04 wt% for La, Ce, Nd, and Yb. On-peak WDS X-ray mapping of Sc, Zr, Y, and Dy in ACM-3 (Fig. 3) was carried out at 15 kV and 100 nA, counting for 500 ms per pixel. The 250 × 320 pixel maps were collected using a 0.5 μm step size and without a background correction.

The empirical formula of type kangite as analyzed by EPMA, based on three O atoms, is $[(Sc_{0.53}Al_{0.19}Y_{0.07}V_{0.02}Gd_{0.01}Dy_{0.01}Er_{0.01})^{3+}_{\Sigma 0.84}(Ti_{0.63}Zr_{0.13}Si_{0.04})^{4+}_{\Sigma 0.80}(Mg_{0.11}Ca_{0.10}Fe_{0.02})^{2+}_{\Sigma 0.23}\square_{0.13}]_{\Sigma 2.00}O_3$, where the oxidation states of Ti, V, and Fe are assumed to be 4+, 3+, and 2+, respectively. Oxygen analyses by EPMA (at 15 kV and 25 nA, using a LDE1 crystal for O$K\alpha$ measurement and synthetic TiO_2 as standard) in both kangite and perovskite support Ti^{4+} (vs. Ti^{3+}) in kangite, as shown in Table 1 where leftover O in kangite (also perovskite) is roughly one standard deviation of the measured oxygen content when all Ti is assigned to 4+. If all Ti is assumed to be 3+, then leftover oxygen in kangite is 3.4 wt% (i.e., an order of magnitude higher than the analytical error). We cannot reject the possibility that minor Ti is trivalent as 8% of the Ti in the kangite analysis in Table 1 would be Ti^{3+} if the measured oxygen content is used to calculate Ti^{3+}/Ti^{4+} (contamination from nearby davisite, which is Ti^{3+}-enriched (Ma and Rossman 2009b), does not significantly affect this calcula-

TABLE 1. Mean electron microprobe analytical results for type kangite, associated perovskite, spinel, and host davisite

Constituent	Kangite	Perovskite	Davisite next to kangite and perovskite	Davisite near the edge	Spinel
wt%	n = 7*	n = 6	n = 6	n = 2	n = 6
TiO_2	36.6(4)†	51.2(3)	8.9(6)	9.2(7)	0.42(2)
Sc_2O_3	26.4(5)	0.8(2)	15(1)	9(1)	0.05(1)
ZrO_2	11.3(3)	0.13(5)	2.1(5)	1.1(3)	b.d.
Al_2O_3	7.0(2)	0.84(9)	22(2)	19.1(5)	65.75(7)
Y_2O_3	5.4(1)	6.3(1)	0.8(1)	0.68(3)	b.d.
CaO	3.9(2)	31.3(2)	23.2(4)	23.70(2)	0.15(2)
MgO	3.14(6)	b.d.‡	2(1)	5.4(5)	21.2(1)
SiO_2	1.7(4)	b.d.	25(2)	31.1(7)	b.d.
V_2O_3	1.31(4)	0.64(4)	0.53(2)	0.52(4)	0.38(1)
FeO	0.8(6)	0.61(2)	0.40(7)	0.43(7)	11.22(7)
Cr_2O_3	0.09(2)	b.d.	b.d.	0.03(1)	0.30(1)
Dy_2O_3	1.8(1)	3.1(1)	0.30(7)	0.25(4)	n.a.§
Er_2O_3	0.92(5)	1.00(5)	0.10(5)	b.d.	n.a.
Gd_2O_3	0.60(4)	2.52(7)	0.18(9)	0.14(2)	n.a.
Ho_2O_3	0.40(2)	0.48(7)	b.d.	b.d.	n.a.
Tb_2O_3	0.18(7)	0.40(6)	b.d.	b.d.	n.a.
ThO_2	0.04(2)	0.40(6)	b.d.	b.d.	n.a.
O‖	−0.3(2)	−0.3(2)			
Total	101.28	99.42	100.51	100.65	99.47

* Number of analyses.
† Numbers in parentheses represent one standard deviation of the mean for the n analyses conducted on the phase.
‡ Below detection. Detection limits at 99% confidence are Mg 0.09 wt%, Si 0.08%, Cr 0.07%, Zr 0.05%, Y 0.06%, Si 0.02%, Er 0.10%, Ho 0.09%, Tb 0.08%, Th 0.03%.
§ Not analyzed.
‖ Difference between oxygen measured by EPMA and value obtained from elemental concentrations of cations as determined by EPMA in which a single valence (listed in the left-hand column) has been assumed for each of the oxides. The quoted uncertainty reflects only the analytical error on the oxygen analysis.

tion). Nevertheless, EPMA analyses clearly indicate that Ti in kangite is dominantly 4+. We cannot be certain of the valence for Fe or V because the concentrations are too low. Some of the Fe in kangite could be ferric as alloys in Allende refractory inclusions were often oxidized to magnetite during low-temperature metasomatism (Blum et al. 1989) and some of the V could be divalent as roughly half of the V in clinopyroxene and spinel from Ca-,Al-rich inclusions from Allende is V^{2+} (Simon et al. 2007; Paque et al. 2010). Changing the assigned valences for Fe and/or V has a negligible effect on the inferred crystallographic properties and no effect on the nomenclature of kangite or our conclusions regarding origin. The apparent Si content in kangite is likely derived from the surrounding davisite, because of the small grain size. If all Si and associated cations in the form of surrounding davisite are removed, kangite shows a formula of $[(Sc_{0.54}Al_{0.16}Y_{0.07}V_{0.03}Gd_{0.01}Dy_{0.01}Er_{0.01})^{3+}_{\Sigma 0.83}(Ti_{0.66}Zr_{0.13})^{4+}_{\Sigma 0.79}(Mg_{0.11}Ca_{0.06}Fe_{0.02})^{2+}_{\Sigma 0.19}\square_{0.19}]_{\Sigma 2.00}O_3$. Kangite is much more Ti- and Sc-rich than previously reported zirconias and is more Sc-rich than panguite (Fig. 4). Based on EPMA, kangite exhibits an ultra-refractory rare earth element (REE) pattern in which most of the heavy REE (HREE) are greatly enriched relative to the LREE and Yb is depleted relative to the other HREE (concentrations of La, Ce, Nd, Sm, and Yb are all below EPMA detection limits, 0.03–0.04 wt%) (Fig. 5). The general formula for kangite is $(Sc,Ti,Al,Zr,Mg,Ca,\square)_2O_3$, or $(Sc,Ti,Al,Zr,Mg,Ca)_{1.8}O_3$, where Sc^{3+} is the dominant trivalent component and the trivalent cations are dominant in the cation sites without indications for cation ordering. The IMA-approved dominant-valency rule (Hatert and Burke 2008) is applied here to designate this oxide as a new Sc mineral. The ideal end-member formula is Sc_2O_3.

Kangite occurs within an aggregate of 2–12 μm diameter crystals of davisite, whose Sc_2O_3 content ranges from as high as 17.66 wt% in portions of the inclusion near the spray of kangite and perovskite crystals, to as low as 8.05 wt% near the inclusion-matrix boundary and in the two lower lobes of the inclusion (the lobe containing the "spinel" label in Fig. 1 and the smaller lobe above and to the left of it; see also the Sc X-ray map in Fig. 3). Davisite in the central region surrounding kangite and perovskite has a mean composition of $Ca_{0.98}(Sc_{0.52}Ti^{3+}_{0.17}Mg_{0.14}Ti^{4+}_{0.09}Zr_{0.04}V^{3+}_{0.02}Y_{0.02}Al_{0.01}Fe^{2+}_{0.01})(Si_{1.00}Al_{1.00})O_6$, where partitioning of Ti^{3+} and Ti^{4+} is based on a stoichiometric formula unit containing 4.00 cations and 6 O atoms. High-Sc davisite is HREE enriched (LREE are below detection limits) but concentrations are a factor of several to an order of magnitude lower than in perovskite and kangite. Low-Sc davisite is also lower in Zr and HREE than high-Sc crystals, showing an average formula of $Ca_{0.98}(Sc_{0.30}Ti^{3+}_{0.19}Mg_{0.31}Ti^{4+}_{0.08}Al_{0.07}Zr_{0.02}V^{3+}_{0.02}Y_{0.01}Fe^{2+}_{0.01})(Si_{1.20}Al_{0.80})O_6$. If kangite and nearby davisite equilibrated with each other (although this may not have been the case, as discussed below), the compositions (Table 1; Fig. 3) imply that Zr, V, Y, and the REE are strongly partitioned into kangite relative to davisite and Ca and, to a lesser extent, Al in davisite relative to kangite; the Ti oxide panguite displays similar partitioning relationships with associated davisite (Ma et al. 2012). Note that about two-thirds of the Ti in davisite is inferred to be trivalent while coexisting kangite contains little if any Ti^{3+}. One possible interpretation of this observation is that kangite strongly preferred Ti^{4+} and discriminated against Ti^{3+} relative to davisite. However, we argue below that kangite is the low-temperature oxidation product of a high-temperature Ti^{3+}-rich phase. Relative concentrations of cations were not significantly affected but the additional oxygen was accommodated through the transformation of Ti^{3+} to Ti^{4+}.

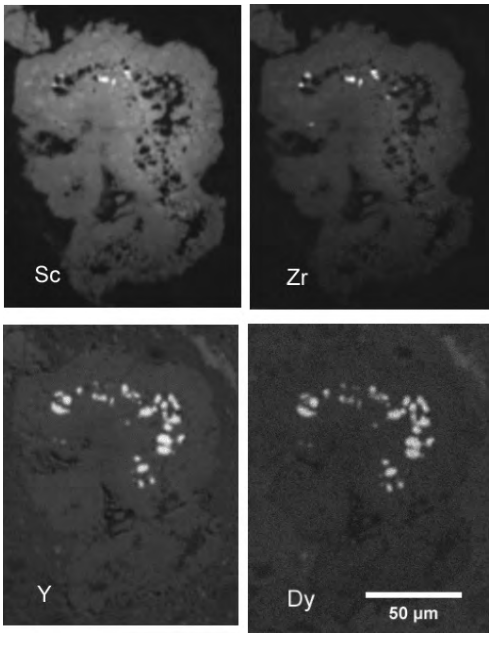

FIGURE 3. Sc, Zr, Y, and Dy X-ray maps of ultra-refractory inclusion ACM-3.

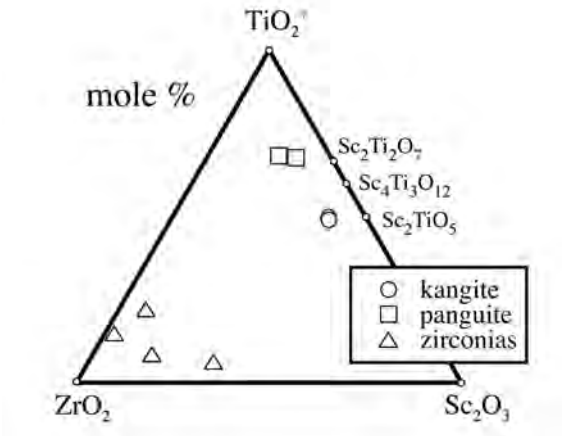

FIGURE 4. Compositions in mol% of meteoritic Sc-,Zr-enriched oxides in terms of the ternary Sc_2O_3-TiO_2* (where all Ti is computed as TiO_2)-ZrO_2. These three oxides account for 80–97% of cations in the zirconias and 70–74% of the cations in kangite and panguite, the balance being mostly Al, Ca, Mg, and Y. Data are taken from Noonan et al. (1977), Lovering et al. (1979), Hinton et al. (1988), Weber and Bischoff (1994), Ma et al. (2012), and this study.

Perovskite in the kangite type example (Figs. 1–2) is Y-rich (Table 1) but Zr-poor (~0.1 wt%), with a formula of $(Ca_{0.82}Y_{0.08}Dy_{0.03}Gd_{0.02}Sc_{0.02}Fe_{0.01}Er_{0.01}V_{0.01})(Ti_{0.94}Al_{0.02})O_3$. As in kangite, the perovskite is HREE enriched with concentrations of LREE below EPMA detection limits (Table 1; Fig. 5). Perovskite with similar REE abundances described by Weber and Bischoff (1994) is relatively Zr-rich (ZrO_2 ~4 wt%). Associated spinel (Fig. 2) is Fe-rich (11.22 wt% FeO) with 0.42 wt% TiO_2, 0.38 wt% V_2O_3, and 0.30 wt% Cr_2O_3 (Table 1), showing a formula of $(Mg_{0.79}Fe_{0.24})(Al_{1.95}Ti_{0.01}V_{0.01}Cr_{0.01})O_4$. We note that stoichiometry considerations require $Fe^{2+} >> Fe^{3+}$ for this phase (i.e., the spinel is hercynitic). The valence state of Ti in the spinel, which can be either Ti^{3+}- or Ti^{4+}-enriched, at least in type B1 inclusions (Paque et al. 2010), is unknown. Overall, V-Ti-Cr concentrations are higher than for most reported spinels from meteoritic inclusions in carbonaceous chondrites (e.g., Connolly and Burnett 1999; Connolly et al. 2003), but they are not diagnostic because similarly enriched compositions, although rare, are occasionally encountered in wide variety of inclusion types including fine-grained (Krot et al. 2004), compact type A (Srinivasan et al. 2000), fluffy type A (Allen et al. 1978), and type B1 inclusions (Wark and Lovering 1982; El Goresy et al. 1985; Armstrong et al. 1987).

CRYSTALLOGRAPHY

EBSD and synchrotron micro-Laue diffraction

EBSD analyses at a submicrometer scale were performed on the vibration-polished section using methods described in Ma and Rossman (2008a, 2009a). An HKL (now Oxford) EBSD system on a Zeiss 1550VP scanning electron microscope was used for these measurements and operated at 20 kV and 6 nA in a focused beam configuration with a 70° tilted stage and variable pressure (25 Pa) mode, which allows the study of uncoated specimens. EBSD patterns of the kangite grains were indexed against structures of synthetic Sc_2O_3 (Schleid and Meyer 1989), $ScTiO_3$ (Shafi et al. 2012), Sc_2TiO_5 (Kolitsch and Tillmanns 2003), Ti_2O_3 (Vincent et al. 1980), and perovskite $CaTiO_3$ (Liu and Liebermann 1993), and the minerals panguite $(Ti^{4+},Sc,Al,Mg,Zr,Ca)_{1.8}O_3$ (IMA 2010-057; Ma et al. 2012), and tazheranite $(Zr,Ti,Ca)O_{1.75}$ (cubic zirconia; Rastsvetaeva et al. 1998). Among these, the patterns can be indexed using a bixbyite-type structure (Sc_2O_3, $ScTiO_3$), a bixbyite-type related structure (panguite), and a fluorite-type structure (tazheranite). Since the bixbyite structure can be derived from a fluorite-structured oxide through a systematic removal of O atoms, it follows that the EBSD data suggest a fluorite- or defective fluorite-structure.

Synchrotron micro-Laue diffraction on one kangite domain was carried out at the 34ID-E undulator beamline of the Advanced Photon Source in the Argonne National Laboratory using a 250 × 400 nm^2 polychromatic X-ray beam and an array of Perkin-Elmer amorphous Si area detectors, using methods described in detail by Ma et al. (2012) in our study of the newly discovered Sc-bearing Ti-oxide panguite. An energy scan (energy range 16 to 27 keV, 1 eV steps) of the primary beam yielded a set of 16 reflections, which were used for a reverse Monte Carlo optimization (Endeavor 1.4; Puetz et al. 1999) with the Sc_2O_3 C-type (bixbyite-type) structure as the initial configuration. The rMC optimization converged to $R_{Bragg} = 0.079$ for the cubic bixbyite-type structure (see Deposit Table[1]). Subsequently we used SHELXL

[1]Deposit item AM-13-064, Deposit Table and CIF. Deposit items are available two ways: For a paper copy contact the Business Office of the Mineralogical Society of America (see inside front cover of recent issue) for price information. For an electronic copy visit the MSA web site at http://www.minsocam.org, go to the *American Mineralogist* Contents, find the table of contents for the specific volume/issue wanted, and then click on the deposit link there.

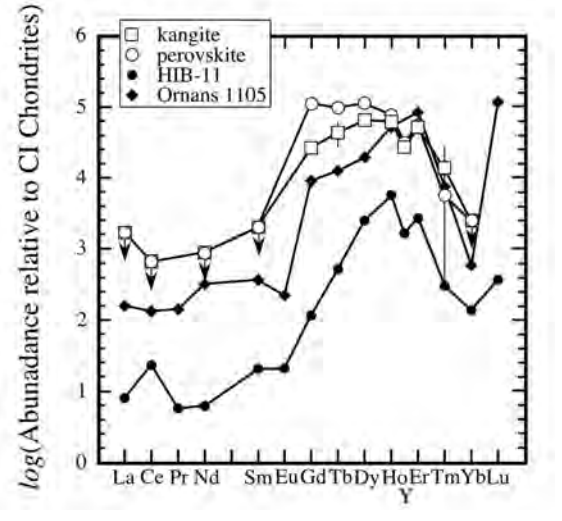

FIGURE 5. Abundance of REE and Y relative to CI chondrites (Anders and Grevesse 1989) in kangite and perovskite from ACM-3. Error bars for analyses from this study are standard deviations on multiple analyses where larger than the symbols. Downward pointing arrows indicate maximum concentrations set at the detection limit for our EPMA analyses. Also shown are the REE patterns for an ultra-refractory cluster of oxides in Ornans inclusion 1105-42 (Davis 1991) and inclusion HIB-11 from Murchison, which consists of perovskite and spinel in a davisite-rich inclusion (Simon et al. 1996). Error bars for literature analyses are not shown.

(Sheldrick 2008) for refinement. Isotropic atomic displacement (U_{iso}) values, site occupancy factors (SOFs) of Sc1, Sc2, and x,y,z coordinates for the cation and oxygen sites are given in Table 2 and CIF deposit[1]. Refinement of the U_{iso} values, SOFs and fractional coordinates was conducted in sequential steps.

Kangite shows a cation-deficient $Ia\bar{3}$ bixbyite-type structure with unit-cell dimension a = 9.842(1) Å, V = 953.3(1) Å^3, and Z = 16. The EBSD pattern (Fig. 6) is an excellent match to the computed EBSD pattern obtained using the cell parameter of the cubic structure from the synchrotron micro-diffraction analysis with resulting mean angular deviations as low as 0.35. X-ray powder-diffraction data (Table 3, in angstroms for Cu$K\alpha_1$, in Bragg-Brentano geometry) were calculated using PowderCell (Kraus and Nolze 1996) version 2.4. Cation-cation distances in kangite are around 2.6% larger than in synthetic Sc_2O_3 (Schleid and Meyer 1989). Isotropic thermal displacement factors of the 8*a* and the 24*d* cations are similar, 0.017 and 0.015 in synthetic Sc_2O_3 (Schleid and Meyer 1989) vs. 0.012 and 0.009 in kangite (Table 2), respectively. However, thermal displacement of oxygen is significantly larger in kangite than in synthetic Sc_2O_3: 0.16 vs. 0.019 Å^{-2}. We relate this observation to another important difference between the structures of kangite and synthetic pure Sc_2O_3. In both kangite and pure Sc_2O_3, cations residing at site 8*a* have six next neighbor anions, although cation-anion distances are 5% shorter in kangite than in pure Sc_2O_3. In synthetic Sc_2O_3, the cation on site 24*d* has sixfold coordination with Sc-O distances ranging from 2.08 to 2.17 Å, as expected for bixbyite-type phases (Wyckoff 1960). In kangite, however, two apices of the 24*d* centered polyhedron are clearly beyond Sc-O bond distances, leaving Sc with an apparent fourfold coordination. The four shortest cation-O distances range from 1.8 to 2.2 Å with the other two at 3.0 and 3.5 Å. Obviously, bond orbital distributions still require a six- to eightfold coordination of the major cations (Sc, Ti, Zr, etc.). These unusual observations can be explained by the high density of cation vacancies in kangite and the fact that site occupancies for the 8*a* and 24*d* sites are quite different. The 24*d* site has only 60% occupancy, whereas the 8*a* site has 80% occupancy. It is therefore likely that cations in the 8*a* site more closely attract O in unit cells for which the 24*d* site is empty than in those for which 24*d* is occupied. In the averaged structure sampled by the micro-Laue measurements, this results in an overall shift of the O-atom position away from the 24*d* site leaving the latter with an apparent incomplete coordination. This interpretation is supported by the unusually large thermal displacement factor of O, which is almost a factor of 10 larger than in pure Sc_2O_3 (see above). In other words, this large thermal displacement factor convolutes the static disorder of O atomic positions in kangite. Such disorder can, in principle, be modeled by partial occupancies of multiple 48*e* sites for O. However, such further refinement would require more unique reflections than are available in our data set.

The structural relationships between kangite and panguite are very interesting because of the similar compositions. Both phases are Ti-,Sc-rich oxides, whose compositions are well expressed using a pseudobrookite-type formula M_3O_5, but they reveal a bixbyite-type (M_2O_3) or related structure. Kangite, which contains more Sc and significantly higher HREE contents, has a bixbyite-type structure, whereas panguite shows a reduction in symmetry from bixbyite-type $Ia\bar{3}$ to *Pbca*. In bixbyite and kangite, the cations assume two Wyckoff sites, 8*a* and 24*d*, whereas the anion resides on the general position 48*e*. The cubic bixbyite structure is related to the structure of panguite by a group-subgroup chain $Ia\bar{3} \rightarrow Ibca \rightarrow Pbca$ where all atoms occupy the general site 8*c* (Aroyo et al. 2006). The reduced crystal symmetry of panguite is the result of lattice relaxation due to the large number of vacancies and large concentration of cations whose ionic radii are smaller than expected for a bixbyite-type structure. This has been discussed in detail in Ma et al. (2012). Kangite has similarly large cation deficiency but a larger concentration of REE elements, all of which establish end-member oxides in the bixbyite structure. It is this higher concentration of large cations that stabilizes the bixbyite structure for kangite. Cooling rates during the formation process may also play a role. However, this can only be assessed by experimental studies on synthetic equivalents of kangite and panguite.

Raman spectroscopy

Raman spectroscopic microanalysis was carried out using a Renishaw M1000 micro-Raman spectrometer system on kangite domains of the sample in polished section, using the methods described in Ma and Rossman (2008a, 2009a). Approximately 5 mW of 514.5 nm laser illumination (at the sample) focused with a 100× objective lens provided satisfactory spectra. The spot size was about 2 μm. The spectrum of kangite is characterized by intense fluorescence features, similar to those of nearby perovskite grains, as shown in Figure 7. The dominant Raman feature of synthetic Sc_2O_3 at 419 cm^{-1} (Ubaldini and Carnasciali 2008) is nearly invisible. The intense fluorescence features are due to significant amounts of fluorescent REE elements in both kangite and perovskite (Table 1). Because features in the Raman spectra arise from intense optical fluorescence due to the REE elements, there are no identifiable Raman shifts and, hence, the spectra provide no information about the crystal structure of the host phase.

Discussion

Kangite is a new Sc-,Ti-rich oxide, (Sc,Ti,Al,Zr,Mg,Ca,□)$_2O_3$,with a $Ia\bar{3}$ bixbyite-type structure, and a new member of the bixbyite group, which already contains bixbyite (Mn_2O_3), avicennite (Tl_2O_3), and yttriaite-(Y) (Y_2O_3). It is the first mineral with a bixbyite-type structure to be found in a meteorite. Kangite also joins various Zr-, Y-, and Sc-rich oxides and silicates, including allendeite, tazheranite, zirconolite, panguite, thortveitite, lakargiite, eringaite, and davisite, that have been reported in refractory inclusions from carbonaceous chondrites (Allen et al. 1980; Hinton et al. 1988; El Goresy et al. 2002; Ma and Rossman 2008b, 2009b; Ma et al. 2009, 2011, 2012; Ma 2011, 2012). Each of these phases is a potential sensor of environment and kangite has the added advantage of being heavy rare earth enriched and, therefore, potentially sensitive to condensation and evaporative processes.

The juxtaposition of kangite, which has little if any Ti^{3+}, within an aggregate of davisite crystals whose Ti is largely trivalent, presents a challenge for understanding the origin of kangite. There are three basic possibilities: (1) kangite formed or equilibrated in an oxidizing environment separate from the reducing environment necessary to produce davisite and was later transported to the

TABLE 2. Atom coordinates

	x/a	*y/b*	*z/c*	SOF	U_{iso}
Sc1	0.25	0.25	0.25	0.767(2)	0.012(3)
Sc2	0.9784(2)	0	0.25	0.590(1)	0.0093(3)
O	0.3207(6)	0.227(5)	–0.44(5)	1	0.16(9)

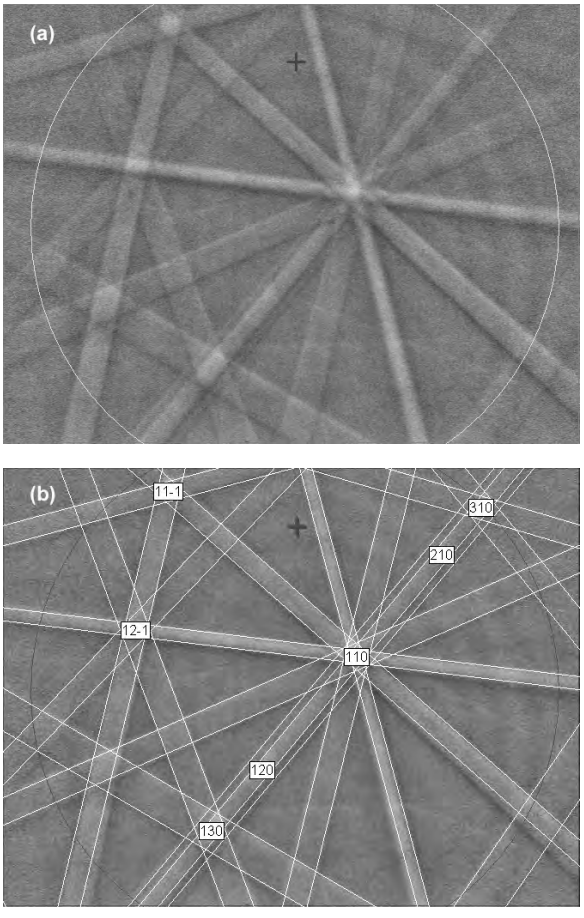

FIGURE 6. (**a**) EBSD pattern of the kangite crystal marked with a cross in Figure 2a. (**b**) The same pattern indexed with the cubic $Ia\bar{3}$ structure obtained by synchrotron micro-Laue diffraction.

davisite (or vice versa); (2) davisite and kangite both form under reducing conditions, but kangite discriminates against Ti^{3+} in much the same way that perovskite, which is also present in this inclusion, does; (3) kangite originally formed as a Ti^{3+}-enriched phase that was incorporated into the davisite aggregate but these original grains were later oxidized at low temperatures (too low to affect the davisite) to form kangite.

Phase equilibria place basic constraints on the stability of a mineral and the conditions under which it may have formed. For kangite, the most relevant binary system under oxidizing conditions is Sc_2O_3-TiO_2 but the phase relations of Sc_2O_3-TiO_x-bearing systems in general and of bixbyite-structured oxides within these systems in particular are poorly constrained. The high-temperature phase diagram of Magunov and Magunov (2002) for the system Sc_2O_3-TiO_2 shows a solubility of only a few mol% TiO_2 in the terminal Sc_2O_3 solid solution (their data constrain it to <10 mol%) with greater amounts of TiO_2 generating Sc_2TiO_5 up to the melting

TABLE 3. Calculated X-ray powder diffraction data for kangite*

h	*k*	*l*	*d* (Å)	I_{rel}†
2	**1**	**1**	**4.0190**	**16**
2	**2**	**2**	**2.8419**	**100**
3	2	1	2.6311	1
4	**0**	**0**	**2.4612**	**10**
4	1	1	2.3204	5
4	2	0	2.2013	1
3	**3**	**2**	**2.0989**	**15**
4	2	2	2.0095	2
4	**1**	**3**	**1.9307**	**75**
5	2	1	1.7974	3
4	**4**	**0**	**1.7403**	**51**
4	3	3	1.6883	3
4	4	2	1.6408	1
6	1	1	1.5970	4
6	0	2	1.5566	1
5	**4**	**1**	**1.5191**	**29**
6	**2**	**2**	**1.4841**	**23**
6	1	3	1.4515	4
4	4	4	1.4210	2
5	4	3	1.3922	2
6	0	4	1.3652	1
7	2	1	1.3397	4
6	4	2	1.3155	1
6	1	5	1.2503	1
8	0	0	1.2306	4
8	1	1	1.2118	2
8	2	0	1.1938	1
6	5	3	1.1767	1
8	2	2	1.1602	1
8	3	1	1.1444	1
6	6	2	1.1293	6
8	0	4	1.1007	2
8	3	3	1.0869	1
8	2	4	1.0739	1
6	5	5	1.0613	2
6	6	4	1.0492	1
7	4	5	1.0374	1
7	6	3	1.0151	2
8	4	4	1.0045	5
9	4	1	0.9942	1
8	5	3	0.9942	2
8	6	0	0.9842	2
7	7	2	0.9745	1
8	2	6	0.9651	4
9	3	4	0.9559	1
10	2	2	0.9471	4
7	6	5	0.9384	1
8	5	5	0.9218	1

* Most intense peaks (I_{rel} ≥ 10) are indicated in bold.
† Relative peak intensity scaled to 100 for the most intense peak.

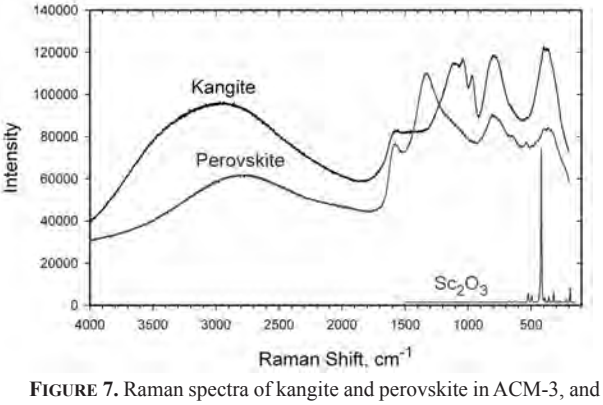

FIGURE 7. Raman spectra of kangite and perovskite in ACM-3, and synthetic Sc_2O_3. The peaks for kangite and perovskite are dominated by optical fluorescence features due to high concentrations of REEs in the crystals so that no Raman shifts can be distinguished.

point of that compound at 1347 °C. Although they did not note it, the compound $Sc_4Ti_3O_{12}$ (e.g., Lyashenko et al. 2004) also appears to be stable in this system at high temperatures. There are also some constraints on phase stabilities for compositions within the quaternary Sc_2O_3-TiO_2-Y_2O_3-ZrO_2 (e.g., Tao and Irvine 2002) but the experimentally examined compositions are far richer in Y+Zr (≥65 mol% of the cations for Tao and Irvine's study) than in kangite (~10%; Fig. 4). Kangite has not been synthesized to our knowledge but many trivalent end-member oxides are known to assume a bixbyite structure, including Sc_2O_3, Y_2O_3, trivalent oxides of the rare earths, and In_2O_3. Available data for Sc_2O_3-TiO_2 imply that a bixbyite structured scandian oxide as TiO_2-rich as kangite (molar Ti/Sc ~1.2) is not a stable high-temperature phase under oxidizing conditions relative to a Sc_2TiO_5- or $Sc_4Ti_3O_{12}$-bearing phase assemblage. This argues against scenario (1) given at the beginning of this section and argues for a low-temperature origin. If kangite is a high-temperature phase produced under oxidizing conditions, then one or more of the other cations present in significant concentrations (i.e., Al, Zr, Mg, and/or Ca) must have stabilized the bixbyite structure.

It is important to consider the possible role of Ti^{3+} in the origin of kangite, both from the perspective of whether or not kangite can accommodate Ti^{3+} (e.g., scenario 2) and what the nature and stability of a Ti^{3+}-enriched precursor would have been (scenario 3). The average ionic radius of trivalent cations in kangite is 0.70 Å and, if Si is removed from the formula in the form of davisite (i.e., all Si in the kangite analysis is due to contamination of the activation volumes for EPMA by the surrounding davisite), then the average ionic radius is 0.67 Å. Moreover, trivalent cations present in significant concentrations (Al, Sc, Y) have ionic radii ranging from 0.53 to 0.89 Å. The ionic radius of Ti^{3+} is 0.67 Å, near the average, which implies that there are no large size-related energetic penalties associated with the substitution of Ti^{3+} into kangite. Thus, scenario (2) is unlikely. Kangite discriminated against Ti^{3+} because there was little or none to be had at the time it formed. Kangite formed (or equilibrated) in an oxidizing environment separate from the one that produced the davisite.

If kangite is the oxidized form of a Ti^{3+}-enriched precursor (scenario 3), then phase relations in the system Sc_2O_3-Ti_2O_3 are pertinent to the origin of the precursor but these are even less well constrained than for Sc_2O_3-TiO_2. Ti_2O_3, which takes on a corundum-type structure ($R\bar{3}c$), can be synthesized with up to 4 mol% Sc_2O_3 (Chandrashekar et al. 1974) and the double oxide $ScTi^{3+}O_3$, which has a bixbyite-type structure, is readily synthesized at high temperatures under reducing conditions (Reid and Sienko 1967). The solubility of Ti_2O_3 in a terminal Sc_2O_3 solution is unknown but, given that bixbyite-type structures tend to be mostly sensitive to ionic radius for a potential substituting cation, it seems likely that the solubility is significantly greater than that of Sc in tistarite (Ti_2O_3). Even these limited observations place an important constraint on the origin of kangite. A kangite precursor could, in principle have been an M_2O_3 oxide but, given the low solubility of Sc in Ti_2O_3, it was not tistarite.

Although there is a paucity of phase equilibrium data for kangite composition oxides and Ti^{3+}-enriched analogs, there is a substantial literature concerning the solubility relationships and energetics of solid solutions of bixbyite-type structured oxides. Systems involving In_2O_3 are the most heavily studied because of their use in energy efficient windows, flat screen panel displays and an assortment of photovoltaics but there are enough data on enough systems (e.g., Busker et al. 1999; Freeman et al. 2000; Saha et al. 2002; Mason et al. 2003; Levy et al. 2007; Hoel et al. 2010) to allow for the expression of some general principles regarding the substitution of cations into a bixbyite structured end-member M_2O_3 oxide such that the $Ia\bar{3}$ space group is retained: (1) for an aliovalent substitution (i.e., a 3+ cation substituting for a 3+ cation), cations with ionic radii similar to those of the host are energetically favored; (2) substitution of a single type of divalent or tetravalent cation for a 3+ host is compensated by oxygen interstitials or cation vacancies (for kangite this would likely be via cation vacancies); (3) co-doping of 4+ and 2+ cations substantially enhances the solubility of both cations relative to the solubility of either by itself; and (4) the solubility of co-doped 4+ and 2+ cations is maximized when the average ionic radius of the two cations approaches that of the host.

Consider a reduced precursor to kangite (scenario 3) in light of the above four principles. We begin with the premise that Si is a contaminant from davisite, although it is possible that Si is soluble in small amounts in kangite. As shown above, removing the Si by subtracting davisite and renormalizing to a 3 oxygen basis leads to the kangite formula: $[(Sc_{0.54}Al_{0.16}Y_{0.07}V_{0.03}Gd_{0.01}Dy_{0.01}Er_{0.01})^{3+}_{\Sigma 0.83}(Ti_{0.66}Zr_{0.13})^{4+}_{\Sigma 0.79}(Mg_{0.11}Ca_{0.06}Fe_{0.02})^{2+}_{\Sigma 0.19}\square_{0.19}]_{\Sigma 2.00}O_3$. This formula has slightly lower Al and Ca (and no Si) than the measured kangite composition as given in Table 1 because these cations are in much greater abundance in davisite than in kangite. There are 0.79 quadrivalent cations in this formula unit but only 0.19 divalent cations, which means that there are far more 4+ cations than can be accommodated through co-doping of 2+ and 4+ cations. This is equivalent to saying that there are far more Ti^{4+} cations than can be accounted for through co-doping. As an end-member model, we assume that all 4+ cations are co-doped with 2+ cations in the kangite precursor and that all remaining Ti in the kangite precursor was trivalent. This yields a formula unit of $[(Ti_{0.61}Sc_{0.53}Al_{0.19}Y_{0.06}V_{0.02}Gd_{0.01}Dy_{0.01}Er_{0.01})^{3+}_{\Sigma 1.44}(Ti_{0.05}Zr_{0.14})^{4+}_{\Sigma 0.19}(Mg_{0.11}Ca_{0.06}Fe_{0.02})^{2+}_{\Sigma 0.19}]_{\Sigma 2.00}O_3$ for the kangite precursor. Note that this phase has an even higher Ti^{+3}/Ti^{+4} ratio (12) than does davisite (2). Of course, intermediate formulas can be constructed in which some fraction of the Ti that is not co-doped with a divalent cation is accommodated as Ti^{4+} in the precursor through cation defects or interstitial oxygen. Ti^{4+} (0.605 Å) has a significantly lower ionic radius than does Sc (0.73 Å) or Ti^{3+} (0.67 Å) but the average ionic radius for a Ca:Ti^{4+} co-doping couple is higher (0.80 Å) than the average ionic radius for the trivalent cations though still smaller than that of Y (0.89 Å), which is present in kangite in similar concentrations. Perhaps Al, which has a much lower ionic radius (0.53 Å) than those of Sc or Ti^{3+}, partially stabilizes the structure for Ca:Ti^{4+} co-doping by reducing the mean ionic radius for the mineral. Connecting the proposed precursor composition to specific redox conditions would require additional experimentation, but we can say that Ti^{3+}-enriched precursors to kangite are consistent with reducing conditions and that they may have formed in an environment similar to or directly related to the one that produced the host davisite. The structure of the kangite precursor is uncertain but the fact that cations of Ti^{3+} ~ Sc^{3+} in the davisite-corrected formula unit given above suggests the possibility that this may have been an $ScTiO_3$ bixbyite-type

phase with considerable solid solution toward various other components. Alternatively, the inferred Ti:Sc ratio is fortuitous and the kangite precursor was a terminal Sc_2O_3 solid solution. Both phases have a bixbyite-type structure. The kangite precursor, which may well have been a high-temperature condensate, was incorporated into the host davisite aggregate but, at a presumably later time, the 0.6 cations of Ti^{3+} on a 3 oxygen basis, that was originally present, was oxidized to form 0.6 cations of Ti^{4+} and the phase transformed into kangite. Shafi et al. (2012) showed that Ti^{3+} in $ScTi^{3+}O_3$ is readily oxidized at low temperatures to form a metastable intermediate with a stoichiometry of $Sc_2Ti^{4+}{}_2O_7$, which has a defect fluorite structure. A similar process may have occurred with the kangite precursor but this phase, having only half the Ti^{3+} present in the end-member $ScTiO_3$ could only be oxidized to an overall M_3O_5 (i.e., pseudobrookite-like) stoichiometry and it therefore assumed or retained the bixbyite structure, as observed for kangite. The oxidation process must have occurred at a sufficiently low temperature so that the kangite, so produced, did not break down to form other, more stable oxides and davisite was unaffected. We can place some constraints on the conditions for this process through a consideration of CAIs in Allende. Based on alloy-oxide equilibria, the alloys in Allende CAIs were oxidized at temperatures in the vicinity of ~500 °C under conditions about a log unit more oxidizing than the iron-wüstite buffer (e.g., Blum et al. 1989). During this event, clinopyroxene was unaffected but iron diffused into the centers of large, 40–60 μm diameter, spinel grains from the core region of an Allende type B inclusion, hundreds of μm from the surface of the CAI (Paque et al. 2007). Spinel in the kangite bearing inclusion described here is very iron rich (11.2 wt% FeO) and it is likely that this Fe was introduced during the Allende metasomatic event. Given the close proximity of kangite crystals (≤20 μm from the surface of the host inclusion), the small grain size (2–12 μm) of the davisite (hence many grain boundaries that could act as fast pathways for diffusion from the external medium outside the inclusion to the surfaces of the kangite precursors), the small grain size of the kangite (1–4 μm grain sizes but not more than ~2 μm thick; see Fig. 2), and the highly ferroan compositions of nearby and kangite-contacting spinel in the same inclusion, it is virtually certain that the kangite precursor would have been exposed to these oxidizing metasomatic conditions. If so, the low concentration of Fe in kangite suggests that the solubility of Fe^{2+} was very low compared to spinel exposed to virtually identical conditions (cf. Table 1). This is consistent with the absence of exchangeable Ti^{4+} from other phases during the alteration process that would have been necessary to charge balance the substitution of Fe^{2+} into kangite.

We conclude that kangite most likely formed as the low-temperature oxidation product of a Sc-,Ti^{3+}-enriched oxide that formed under reducing conditions, presumably as a condensate and probably with a bixbyite-type structure. Note that this high-temperature precursor, were it to be found, would be a new mineral. It would not be kangite because the cation concentration of Ti^{3+} > Sc, and it would not be tistarite because it would have a different structure. This reduced kangite precursor was incorporated into an aggregate of davisite crystals along with small amounts of perovskite and spinel, and it was later oxidized to form kangite. It is possible that the oxidation event occurred prior to incorporation into the davisite aggregate (i.e., the grains arrived as kangite crystals), but the most straightforward scenario is one in which the same metasomatic event that introduced iron into spinels, including the ones shown in Figures 1 to 2, and oxidized metal in Allende CAIs, also caused in situ oxidation of the kangite precursor. If so, the composition of the kangite, except for oxygen and possibly Fe, approximates that of the original precursor and, because there were ≤0.6 cations of Ti^{3+} per 3 O atoms in the original crystals, oxidation yielded a roughly M_3O_5 stoichiometry and a bixbyite-type structure was retained.

Although we have emphasized the origin of kangite in this discussion, it is also important to place the proposed Ti^{3+}-enriched precursor into a broader cosmochemical context. Both kangite and perovskite in the inclusion described in this study are highly enriched in HREE (Fig. 5), and this provides a key to understanding their origin. In general, ultra-refractory inclusions are characterized by extraordinarily high HREE/LREE ratios and negative Yb anomalies as shown in Figure 5. Only a handful of meteoritic inclusions with ultra-refractory REE patterns have been described (e.g., Davis 1984, 1991; Simon et al. 1996; El Goresy et al. 2002; Uchiyama et al. 2008), but Boynton (1975) proposed their existence before any had been discovered based on thermodynamic modeling of high-temperature condensation. Moreover, the absence of isotopic mass fractionation in Ti and Mg in at least one of these inclusions suggests that the ultra-refractory grains are condensates rather than evaporative residues (Simon et al. 1996). Some meteoritic inclusions (described as Group II) appear to have derived their REE budget via condensation from a reservoir that was depleted in an ultra-refractory component. Group II inclusions are fairly common among CAIs and especially common among fine-grained inclusions (Davis 1991; Hiyagon et al. 2011). Ultra-refractory phases, including perovskite and the kangite precursor from this study, are representatives of solid extracts from high-temperature fractional condensation processes. Although the occurrence of ultra-refractory material as original condensate grains is rare, its effect is often observed through REE patterns of lower temperature condensates that are missing an ultra-refractory component.

Acknowledgments

SEM, EBSD, and EPMA analyses were carried out at the Caltech GPS Division Analytical Facility, which is supported, in part, by NSF Grants EAR-0318518 and DMR-0080065. Synchrotron micro-diffraction was carried out at the 34ID-E beamline of the Advanced Photon Source. Use of the Advanced Photon Source, an Office of Science User Facility operated for the U.S. Department of Energy (DOE) Office of Science by Argonne National Laboratory, was supported by the U.S. DOE under Contract No. DE-AC02-06CH11357. This research was also supported by NASA Cooperative Agreement DE-FC88-01NV14049, NASA OSS Grant NNX09AG40G, and NSF Grant EAR-0947956. We thank A.M. Davis, M. Kimura, R.C. Peterson, and associate editor R.H. Jones for constructive and helpful reviews.

References cited

Allen, J.M., Grossman, L., Davis, A.M., and Hutcheon, I.D. (1978) Mineralogy, textures and mode of formation of a hibonite-bearing Allende inclusion. Proceedings of the 9th Lunar and Planetary Science Conference, 1209–1233.

Allen, J.M., Grossman, L., Lee, T., and Wasserburg, G.J. (1980) Mineralogy and petrography of HAL, an isotopically-unusual Allende inclusion. Geochimica et Cosmochimica Acta, 44, 685–699.

Anders, E. and Grevesse, N. (1989) Abundances of the elements. Geochimica et Cosmochimica Acta, 53, 197–214.

Armstrong, J.T. (1995) CITZAF: a package of correction programs for the quantitative electron microbeam X-ray analysis of thick polished materials, thin films, and particles. Microbeam Analysis, 4, 177–200.

Armstrong, J.T., Hutcheon, I.D., and Wasserburg, G.J. (1987) Zelda and company: Petrogenesis of sulfide-rich Fremdlinge and constraints on solar nebula processes.

Geochimica et Cosmochimica Acta, 51, 3155–3173.
Aroyo, M.I., Perez-Mato, J.M., Capillas, C., Kroumova, E., Ivantchev, S., Madariaga, G., Kirov, A., and Wondratschek, H. (2006) Bilbao Crystallographic Server: I. Databases and crystallographic computing programs. Zeitschrift für Kristallographie, 221, 15–27.
Blum, J.D., Wasserburg, G.J., Hutcheon, I.D., Beckett, J.R., and Stolper, E.M. (1989) Origin of opaque assemblages in C3V meteorites: Implications for nebular and planetary processes. Geochimica et Cosmochimica Acta, 53, 543–556.
Boynton, W.V. (1975) Fractionation in the solar nebula: condensation of yttrium and the rare earth elements. Geochimica et Cosmochimica Acta, 39, 569–584.
Busker, G., Chroneos, A., Grimes, R.W., and Chen, I.W. (1999) Solution mechanisms for dopant oxides in yttria. Journal of the American Ceramic Society, 82, 1553–1559.
Chandrashekar, G.V., Van Zandt, L.L., Honig, J.M., and Jayaraman, A. (1974) Electrical properties and the metal-insulator transition in $(Sc_xTi_{1-x})_2O_3$. Physical Review B, 10, 5063–5068.
Clarke, R.S., Jarosewich, E., Mason, B., Nelen, J., Gómez, M., and Hyde, J.R. (1971) The Allende, Mexico, meteorite shower. Smithsonian Contributions to Earth Science, 5, 1–53.
Connolly, H.C. and Burnett, D.S. (1999) A study of the minor element concentrations of spinels from two type B calcium-aluminum-rich inclusions: An investigation into potential formation conditions of calcium-aluminum-rich inclusions. Meteoritics & Planetary Science, 34, 829–848.
Connolly, H.C., Burnett, D.S., and McKeegan, K.D. (2003) The petrogenesis of type B1 Ca-Al-rich inclusions: The spinel perspective. Meteoritics & Planetary Science, 38, 197–224.
Davis, A.M. (1984) A scandalously refractory inclusion in Ornans. Meteoritics, 19, 214.
——— (1991) Ultrarefractory inclusions and the nature of the group II REE fractionation. Meteoritics, 26, 330.
El Goresy, A., Armstrong, J.T., and Wasserburg, G.J. (1985) Anatomy of an Allende coarse-grained inclusion. Geochimica et Cosmochimica Acta, 49, 2433–2444.
El Goresy, A., Zinner, E., Matsunami, S., Palme, H., Spettel, B., Lin, Y., and Nazarov, M. (2002) Efremovka 101.1: A CAI with ultra-refractory REE patterns and enormous enrichments of Sc, Zr, and Y in fassaite and perovskite. Geochimica et Cosmochimica Acta, 66, 1459–1491.
Freeman, A.J., Poeppelmeier, K.R., Mason, T.O., Chang, R.P.H., and Marks, T.J. (2000) Chemical and film strategies for new transparent conducting oxides. MRS Bulletin, 25, 45–51.
Hatert, F. and Burke, E.A.J. (2008) The IMA-CNMNC dominant-constituent rule revisited and extended. Canadian Mineralogist, 46, 717–728.
Hinton, R.W., Davis, A.M., Scatena-Wachel, D.E., Grossman, L., and Draus, R.J. (1988) A chemical and isotopic study of hibonite-rich refractory inclusions in primitive meteorites. Geochimica et Cosmochimica Acta, 52, 2573–2598.
Hiyagon, H., Yamakawa, A., Ushikubo, T., Lin, Y., and Kimura, M. (2011) Fractionation of rare earth elements in refractory inclusions from the Ningqiang meteorite: Origin of positive anomalies in Ce, Eu, and Yb. Geochimica et Cosmochimica Acta, 75, 3358–3384.
Hoel, C.A., Gaillard, J.-F., and Poeppelmeier, K.R. (2010) Probing the local structure of crystalline ZITO: $In_{2-2x}Sn_xZn_x$ ($x \leq 0.4$) Journal of Solid State Chemistry, 183, 761–768.
Kolitsch, U. and Tillmanns, E. (2003) Sc_2TiO_5, an entropy-stabilized pseudobrookite-type compound. Acta Crystallographica, E59, i36–i39.
Kraus, W. and Nolze, G. (1996) POWDER CELL—a program for the representation and manipulation of crystal structures and calculation of the resulting X-ray powder patterns. Journal of Applied Crystallography, 29, 301–303.
Krot, A.N., MacPherson, G.J., Ulyanov, A.A., and Petaev, M.I. (2004) Fine-grained, spinel-rich inclusions from the reduced CV chondrites Efremovka and Leoville: I. Mineralogy, petrology, and bulk chemistry. Meteoritics & Planetary Science, 39, 1517–1553.
Levy, M.R., Stanek, C.R., Chroneos, A., and Grimes, R.W. (2007) Defect chemistry of doped bixbyite oxides. Solid State Sciences, 9, 588–593.
Liu, X. and Liebermann, R.C. (1993) X-ray powder diffraction study of $CaTiO_3$ perovskite at high temperatures. Physics and Chemistry of Minerals, 20, 171–175.
Lovering, J.F., Wark, D.A., and Sewell, D.K.B. (1979) Refractory oxide, titanate, niobate and silicate accessory mineralogy of some type B Ca-Al-rich inclusions in the Allende meteorite. Lunar and Planetary Science, 10, 745–746.
Lyashenko, L.P., Kolbanev, I.V., Shcherbakova, L.G., Knerel'man, E.I., and Davydova, G.I. (2004) Effect of nonequilibrium state on phase relations in the system TiO_2-Sc_2O_3 (40–50 mol% Sc_2O_3). Inorganic Materials, 40, 833–839.
Ma, C. (2011) Discovery of meteoritic lakargiite ($CaZrO_3$), a new ultra-refractory mineral from the Acfer 094 carbonaceous chondrite. Meteoritics & Planetary Science, 46 (S1), A144.
——— (2012) Discovery of meteoritic eringaite, $Ca_3(Sc,Y,Ti)_2Si_3O_{12}$, the first solar garnet? Meteoritics & Planetary Science, 47 (S1), A256.
Ma, C. and Rossman, G.R. (2008a) Barioperovskite, $BaTiO_3$, a new mineral from the Benitoite Mine, California. American Mineralogist, 93, 154–157.
——— (2008b) Discovery of tazheranite (cubic zirconia) in the Allende meteorite. Geochimica et Cosmochimica Acta, 72, 12S, A577.
——— (2009a) Tistarite, Ti_2O_3, a new refractory mineral from the Allende meteorite. American Mineralogist, 94, 841–844.
——— (2009b) Davisite, $CaScAlSiO_6$, a new pyroxene from the Allende meteorite. American Mineralogist, 94, 845–848.
Ma, C., Beckett, J.R., and Rossman, G.R. (2009) Allendeite and hexamolybdenum: Two new ultra-refractory minerals in Allende and two missing links. Lunar and Planetary Science 40, Abstract 1402.
Ma, C., Beckett, J.R., Tschauner, O., and Rossman, G.R. (2011) Thortveitite ($Sc_2Si_2O_7$), the first solar silicate? Meteoritics & Planetary Science, 46 (S1), A144.
Ma, C., Tschauner, O., Beckett, J.R., Rossman, G.R., and Liu, W. (2012) Panguite, $(Ti^{4+},Sc,Al,Mg,Zr,Ca)_{1.8}O_3$, a new ultra-refractory titania mineral from the Allende meteorite: Synchrotron micro-diffraction and EBSD. American Mineralogist, 97, 1219–1225.
Magunov, R.L. and Magunov, I.R. (2002) The system Sc_2O_3-TiO_2. Ukrainian Journal of Chemistry, 68, 85–88 (in Russian).
Mason, T.O., Kammler, D.R., Ingram, B.J., Gonzalez, G.B., Young, D.L., and Coutts, T.J. (2003) Key structural and defect chemical aspects of Cd-In-Sn-O transparent conducting oxides. Thin Solid Films, 445, 186–192.
Noonan, A.F., Nelen, J., Fredriksson, K., and Newbury, D. (1977) Zr-Y oxides and high-alkali glass in an amoeboid inclusion from Ornans. Meteoritics, 12, 332–333.
Paque, J.M., Burnett, D.S., and Beckett, J.R. (2007) Zoning patterns of Fe and V in spinel from a type B Ca-Al-rich inclusion: Constraints on subsolidus thermal history. Meteoritics & Planetary Science, 42, 899–912.
Paque, J.M., Sutton, S.R., Burnett, D.S., Beckett, J.R., and Simon, S.B. (2010) An intimate mix of highly oxidizing and highly reducing environments: relict spinel determined by XANES in a partially melted Allende Ca-Al-rich inclusion. Lunar and Planetary Science 41, Abstract 1391.
Puetz, H., J.C. Schön, J.C., and Jansen, M. (1999) Combined method for *ab initio* structure solution from powder diffraction data. Journal of Applied Crystallography, 32, 864–870.
Rastsvetaeva, R.K., Pushcharovskii, D. Yu., Spiridonov, E.M., and Gekimyants, V.M. (1998) Tazheranite and calzirtite: structural-mineralogical similarity and distinction. Doklady Akademii Nauk SSSR, 359, 529–531.
Reid, A.F., and Sienko, M.J. (1967) Scandium titanite and vanadite, $ScTiO_3$ and $ScVO_3$. Inorganic Chemistry, 6, 521–524.
Saha, D., Das Sharma, A., Sen, A., and Maiti, H.S. (2002) Preparation of bixbyite phase $(Mn_xFe_{1-x})_2O_3$ for NTC thermistor applications. Materials Letters, 55, 403–406.
Shafi, S.P., Hernden, B.C., Cranswick, L.M.D., Hansen, T.C., and Bieringer, M. (2012) Topotactic oxidation pathway of $ScTiO_3$ and high-temperature evolution of $ScTiO_{3.5}$ and $Sc_4Ti_3O_{12}$-type phases. Inorganic Chemistry, 51, 1269–1277.
Schleid, T. and Meyer, G. (1989) Single crystals of rare earth oxides from reducing halide melts. Journal of the Less-Common Metals, 149, 73–80.
Sheldrick, G.M. (2008) A short history of SHELX. Acta Crystallographica, A64, 112–122.
Simon, S.B., Davis, A.M., and Grossman, L. (1996) A unique ultrarefractory inclusion from the Murchison meteorite. Meteoritics & Planetary Science, 31, 106–115.
Simon, S.B., Sutton, S.R., Grossman, L. (2007) Valence of titanium and vanadium in pyroxene in refractory inclusion interiors and rims. Geochimica et Cosmochimica Acta, 71, 3098–3118.
Srinivasan, G., Huss, G.R., and Wasserburg, G.J. (2000) A petrographic, chemical, and isotopic study of calcium-aluminum-rich inclusions and aluminum-rich chondrules from the Axtell (CV3) chondrite. Meteoritics & Planetary Science, 35, 1333–1354.
Tao, S. and Irvine, J.T.S. (2002) Optimization of mixed conducting properties of Y_2O_3-ZrO_2-TiO_2 and Sc_2O_3-Y_2O_3-ZrO_2-TiO_2 solid solutions as potential SOFC anode materials. Journal of Solid State Chemistry, 165, 12–18.
Ubaldini, A. and Carnasciali, M.M. (2008) Raman characterisation of powder of cubic RE_2O_3 (RE = Nd, Gd, Dy, Tm, and Lu), Sc_2O_3 and Y_2O_3. Journal of Alloys and Compounds, 454, 374–378.
Uchiyama, K., Hiyagon, H., Takahata, N., Sano, Y., Ushikubo, T., Kimura, M., and Hashimoto, A. (2008) ion microprobe analyses of rare earth elements in an extremely ultrarefractory nodule from the Efremovka CV3 chondrite. Lunar and Planetary Science, 39, Abstract 1519.
Vincent, M.G., Yvon, K., and Gruttner, A. (1980) Electron-density studies of metal-metal bonds. I. The deformation density of Ti_2O_3 at 295 K. Acta Crystallographica, A36, 803–808.
Wark, D.A. and Lovering, J.F. (1982) The nature and origin of type B1 and B2 Ca-Al-rich inclusions in the Allende meteorite. Geochimica et Cosmochimica Acta, 46, 2581–2594.
Weber, D. and Bischoff, A. (1994) The occurrence of grossite ($CaAl_4O_7$) in chondrites. Geochimica et Cosmochimica Acta, 58, 3855–3877.
Wyckoff, R.W.G. (1960) Crystal Structures, vol. 2. Interscience Publishers, New York.

Manuscript received July 10, 2012
Manuscript accepted January 26, 2013
Manuscript handled by Rhian Jones

Deposited Item, Ma et al.: Kangite, a new scandia mineral, AM-13-064, MayJune American Mineralogist 2013.

List of observed and calculated normalized structure factor moduli of unique reflections.*.

h	*k*	*l*	F_o^2	F_c^2	$\sigma(F^2)$/su	F_c/F_c(max)	Resolution (Å)
2	6	8	92916.11	56643.00	1.77	0.575	0.97
4	4 10	52273.38	41034.36	0.97		0.489	0.86
0	6 10	27150.91	32576.42	0.93		0.436	0.84
0	0 10	55806.35	56775.83	0.17		0.576	0.98
4	4	8	168947.70	171334.06	0.14	1.000	1.00

*R_1 = 0.084 for 5 unique reflections after merging; $wR2$ = 0.139, GooF 0.875 (Sheldrick 2008).

Deposited Item, Ma et al.: Kangite, a new scandia mineral, AM-13-064, MayJune
American Mineralogist 2013.

```
#\#CIF_1.1

#  CIF produced by WinGX routine CIF_UPDATE
#  Created on 2012-01-24 at 16:25:09
#  Using CIFtbx version 2.6.2 16 Jun 1998

#  Dictionary name : cif_core.dic
#  Dictionary vers : 2.4
#  Request file    : c:\wingx\files\archive.reqdat
#  CIF files read  : Kangite.cif

#------------------ SECTION 1. GLOBAL INFORMATION ---------------------------#

data_global

#------------------ AUDIT DETAILS -------------------------------------------#

_audit_creation_date            2012-01-24
_audit_creation_method          'WinGX routine CIF_UPDATE'
_audit_conform_dict_name        cif_core.dic
_audit_conform_dict_version     2.4
_audit_conform_dict_location    ftp://ftp.iucr.org/pub/cif_core.dic
_audit_update_record            ?

#------------------ AUTHOR DETAILS ------------------------------------------#

# Name and address of author for correspondence

_publ_contact_author_name      'Tschauner, Oliver'
_publ_contact_author_address
;
Department of Geoscience
University of Nevada Las Vegas
Las Vegas
Nevada, USA
;
_publ_contact_author_email       olivert@physics.unlv.edu
_publ_contact_author_fax         '01(702)8954064'
_publ_contact_author_phone       '01(702)8951716'


# Insert blank lines between references

_publ_section_references
;
enCIFer: Allen, F. H., Johnson, O., Shields, G. P., Smith, B. R. & Towler,
M. (2004). J. Appl. Cryst. 37, 335-338.

Endeavour: H. Putz, J.C. Sch¿on, M. Jansen (1999). J. Appl. Cryst. 32, 864-870.

SHELX Sheldrick, G. M. (2008). Acta Cryst. A64, 112-122.
```

UnitCell: T J B Holland and S A T Redfern (1997). Mineralogical Magazine 61: 65-77.

WinGX: Farrugia, L. J. (1999). J. Appl. Cryst. 32, 837-838.

;

#------------------ SECTION 2. COMPOUND(S) DETAILS -------------------------#

data_scandiarfb

_audit_creation_date   2012-01-24T16:25:09-00:00
_audit_creation_method   'WinGX routine CIF_UPDATE'
_audit_conform_dict_name   cif_core.dic
_audit_conform_dict_version   2.4
_audit_conform_dict_location   ftp://ftp.iucr.org/pub/cif_core.dic
_publ_requested_category   FI

#--#
CHEMICAL INFORMATION
#--#

_chemical_formula_sum   'Sc20.296 O48'
_chemical_formula_weight   1680.396

#--#
UNIT CELL INFORMATION
#--#

_symmetry_space_group_name_H-M   'I a -3'
_symmetry_space_group_name_Hall   -I_2b_2c_3
_symmetry_Int_Tables_number   206
loop_
    _symmetry_equiv_pos_as_xyz
x,y,z
z,x,y
y,z,x
-y,0.500-z,x
z,-x,0.500-y
0.500-y,z,-x
-z,0.500-x,y
0.500-z,x,-y
y,-z,0.500-x
-x,0.500-y,z
x,-y,0.500-z
0.500-x,y,-z
-x,-y,-z
-z,-x,-y
-y,-z,-x
y,0.500+z,-x
-z,x,0.500+y
0.500+y,-z,x
z,0.500+x,-y
0.500+z,-x,y
-y,z,0.500+x

```
x,0.500+y,-z
-x,y,0.500+z
0.500+x,-y,z

_cell_length_a                         9.8415(10)
_cell_length_b                         9.8415(10)
_cell_length_c                         9.8415(10)
_cell_angle_alpha                      90
_cell_angle_beta                       90
_cell_angle_gamma                      90
_cell_volume                           953.2(3)

#------------------------------------------------------------------------------#
#                    CRYSTAL INFORMATION                                       #
#------------------------------------------------------------------------------#


#------------------------------------------------------------------------------#
#                    ABSORPTION CORRECTION                                     #
#------------------------------------------------------------------------------#

_exptl_absorpt_correction_type          none

#------------------------------------------------------------------------------#
#                    DATA COLLECTION                                           #
#------------------------------------------------------------------------------#
#Laue diffraction at APS synchrotron beamline 34-IDE with
#250x400 nm2 beam, subsequent energy scan from 16.5 to 24.0 keV with 3 eV step

#------------------------------------------------------------------------------#
#                    COMPUTER PROGRAMS USED                                    #
#------------------------------------------------------------------------------#
# Endeavour 1.7, UnitCell, Shelxl

#------------------------------------------------------------------------------#
#                    STRUCTURE SOLUTION
#------------------------------------------------------------------------------#
# see Ma et al."Kangite, (Sc,Ti,Al,Zr,Mg,Ca,\\square)2O3, a new
# ultra-refractory scandia mineral from the Allende meteorite:
# Synchrotron micro-diffraction and EBSD", submitted to Am. Min. and
# "Panguite, (Ti4+,Sc,Al,Mg,Zr,Ca)1.8O3, a new refractory mineral
# from the Allende meteorite: Synchrotron micro-diffraction and EBSD"
# Am. Min. msc # 4027

#------------------------------------------------------------------------------#
#                    REFINEMENT INFORMATION                                    #
#------------------------------------------------------------------------------#
# see Ma et al."Kangite, (Sc,Ti,Al,Zr,Mg,Ca,\\square)2O3, a new
# ultra-refractory scandia mineral from the Allende meteorite:
# Synchrotron micro-diffraction and EBSD", submitted to Am. Min. and
# "Panguite, (Ti4+,Sc,Al,Mg,Zr,Ca)1.8O3, a new refractory mineral
# from the Allende meteorite: Synchrotron micro-diffraction and EBSD"
# Am. Min. msc # 4027
```

```
#--------------------------------------------------------------------------#
#                    ATOMIC TYPES, COORDINATES AND THERMAL PARAMETERS      #
#--------------------------------------------------------------------------#

loop_
    _atom_type_symbol
Sc
O

loop_
    _atom_site_label
    _atom_site_type_symbol
    _atom_site_fract_x
    _atom_site_fract_y
    _atom_site_fract_z
    _atom_site_U_iso_or_equiv
    _atom_site_adp_type
    _atom_site_occupancy
    _atom_site_symmetry_multiplicity
    _atom_site_calc_flag
SC1 Sc 0.25 0.25 0.25 0.767(2) Uiso 0.012(3) 8 d
SC2 Sc 0.9764(2) 0 0.25 0.590(1) Uiso 0.0093(3) 24 d
O O 0.3207(6) 0.227(5) -0.44(5) 1 Uiso 0.16(9) 48 d


#--------------------------------------------------------------------------#
#                    MOLECULAR GEOMETRY                                    #
#--------------------------------------------------------------------------#

# END of CIF
```